

# Horizontal rotation signals detected by “G-Pisa” ring laser for the $M_w=9.0$ , March 2011, Japan earthquake

J. Belfi<sup>1</sup>    N. Beverini<sup>1</sup>    G. Carelli<sup>1</sup>    A. Di Virgilio<sup>2</sup>  
 E. Maccioni<sup>1</sup>    G. Saccorotti<sup>3</sup>    F. Stefani<sup>1</sup>  
 A. Velikoseltsev<sup>4</sup>

November 13, 2018

<sup>1</sup> *Department of Physics “Enrico Fermi”, Università di Pisa, Pisa, Italy*

<sup>2</sup> *INFN Section of Pisa, Pisa, Italy*

<sup>3</sup> *INGV - Pisa, Italy and Fondazione Prato Ricerche - Prato, Italy*

<sup>4</sup> *Department of Laser Measurement and Navigation Systems, St.-Petersburg  
 Electrotechnical University, St. Petersburg, Russia*

## Abstract

We report the observation of the ground rotation induced by the  $M_w=9.0$ , 11th of March 2011, Japan earthquake. The rotation measurements have been conducted with a ring laser gyroscope operating in a vertical plane, thus detecting rotations around the horizontal axis. Comparison of ground rotations with vertical accelerations from a co-located force-balance accelerometer shows excellent ring laser coupling at periods longer than 100s. Under the plane wave assumption, we derive a theoretical relationship between horizontal rotation and vertical acceleration for Rayleigh waves. Due to the oblique mounting of the gyroscope with respect to the wave direction-of-arrival, apparent velocities derived from the acceleration / rotation rate ratio are expected to be always larger than, or equal to the true wave propagation velocity. This hypothesis is confirmed through comparison with fundamental-mode, Rayleigh wave phase velocities predicted for a standard Earth model.

## 1 Introduction

High-sensitivity ring laser technology [1] that was developed for geodetic purposes in the past decades (see e.g. [2, 3]) led to the detection of earthquake-induced rotational ground motions far from seismic sources [4, 6, 7, 9] opening a new direction in seismic instrumentation. Using the C-I ring-laser apparatus in Christchurch, New Zealand, these authors were the first to exploit the simple relationship between transverse acceleration and rotation rate assuming plane, horizontally-polarized wave propagation. Nevertheless, their observations were not fully consistent, and were only studied in a narrow frequency band. After then, detailed analyses of co-located measurements of transverse acceleration

and rotation rate were carried out by [10], [11] and [12]. They showed that for several distant large earthquakes the waveforms and amplitudes of translations and rotations matched the expected behavior assuming plane wave theory. In all these past studies, the experimental setup was arranged in order to be sensitive to rotation around the local vertical axis, sometimes also called twist, yaw, spin or torsion in engineering applications.

Rotations around horizontal axis (tilt) couple in a different way with seismic waves. With the exception of a single observation briefly mentioned by [7] for the G0 ring laser at Cashmere, New Zealand, horizontal rotations have not yet been detected systematically using ring-laser systems <sup>1</sup>.

Since June, 2010, a laser gyroscope with a perimeter of 5.20 m, named “G-Pisa”, is operating at the site of the Virgo gravitational wave interferometer, located in Cascina (Pisa, Italy). More details about the present status of the “G-Pisa” apparatus are presented in another paper of this same issue ???. The high sensitivity and low noise level in the spectral range between 1 mHz and 1 Hz makes “G-Pisa” an excellent tool for detecting rotational signals associated with the passage of seismic waves.

Initially, the optical cavity of “G-Pisa” was arranged horizontally. In this configuration, it was sensitive to rotations around the vertical axis and recorded several earthquakes at local and regional distances. Starting on December, 2010, the gyroscope layout was turned, bringing the laser cavity in a vertical plane, in order to be sensitive to rotation motion around an horizontal axis. In this configuration the gyroscope recorded the large  $M_w=9.0$  earthquake which struck the east coast of Honshu, Japan, on 2011 March 11.

This paper focuses entirely on the observations of this catastrophic event and aims at extending the previous studies to the analysis of seismically-induced horizontal ground rotations. The paper is structured as follows. First, we describe the experimental apparatus and present the data set. Then, we use plane-wave theory to derive a theoretical relationship between vertical accelerations and horizontal rotations associated with the propagation of Rayleigh waves. Finally, we use narrow-band correlation analysis to derive apparent Rayleigh waves phase velocities, which are compared to those predicted for a standard Earth model.

## 2 Experimental apparatus

Large-frame laser gyroscopes are the most sensitive devices among the optical rotation sensors. These sensors are free from moving parts and in principle measure rotations completely rejecting linear accelerations and gravitational force and, when properly conditioned, provide excellent low-frequency performances. They consist essentially of gas ring-lasers operating in continuous-wave and single-mode for both the two counter-propagating light beams. When the ring structure is rotating with respect to an inertial frame, the cavity resonance conditions for the two beams are separated in frequency. The optical detection

---

<sup>1</sup>An other ring laser operating with the vertical plane is the PR-1 ring laser. It is mounted on the wall of a laboratory in Department of Physics and Astronomy building at University of Christchurch. However its major goal is the detection of seismically induced rotations in buildings, and it's not operating continuously

of the rotation rate is performed by measuring the beat signal between the two counter-propagating beams outside the cavity. The beat frequency (Sagnac frequency) is related to the rotation rate by a scale factor. For a ring laser with perimeter  $P$ , area vector  $\vec{A} = A\hat{n}$  and wavelength  $\lambda$ , the angular velocity  $\vec{\Omega}$  of its reference frame induces a Sagnac frequency given by:

$$f_S = \frac{4A}{P\lambda} \vec{\Omega} \cdot \hat{n}. \quad (1)$$

Very small rotational signals are observed by using the Earth rotation rate as bias. For a gyro located at the latitude  $\phi$ , the Earth induced frequency shift for the two counterpropagating optical beams can be expressed as:

$$f_S = \frac{8\pi A}{P\lambda T_{l.o.d.}} \sin(\phi + \theta_V) \cos(\theta_N), \quad (2)$$

where  $\theta_V$  and  $\theta_N$  are respectively the angles formed by the laser area normal vector with the local Earth radius and the local meridian while  $T_{l.o.d.}$  is the time length of the sidereal day.

The rotational signal from the earthquake has been detected with the ‘‘G-Pisa’’ gyrolaser, a He-Ne laser emitting on the red line at  $\lambda = 632.8$  nm and operating in a squared cavity  $1.82$  m<sup>2</sup> in area. At the moment of the earthquake event, ‘‘G-Pisa’’ was oriented with the area vector horizontally aligned along the Virgo north-south arm.

A scheme of the experimental setup is sketched in figure 1.

From eq.(2), by considering the latitude of Cascina  $\phi = 43^\circ 37' 53''$ , one obtains an expected mean value for the Sagnac frequency due to the Earth rotation bias, of about 106.2 Hz. The experimentally estimated value differs for few parts per thousand from the expected one. Such a difference has to be attributed to a slight misalignment between the laser plane and the earth radial direction as well as to systematic errors arising from the laser dynamics.

Several seismological instruments are currently operating in different sectors of Virgo’s premise. The most sensitive of these is a Guralp CMG40-T broadband seismometer. Unfortunately, by the time the earthquake occurred, this instrument was operated with a high gain level in order to monitor the micro-seismic activity with high sensitivity, and thus the earthquake signal resulted severely clipped. To the purpose of comparing the translational components of ground motion to the rotational ones, we therefore make use of signals recorded by a tri-axial Episensor ES-T, force-balance accelerometer located at Virgo’s detection bench, some 10 m apart from the ring-laser apparatus.

The Y and X components of the accelerometer are oriented along Virgo’s N arm (see Fig. 1) and perpendicularly to it, respectively. Given the frequency range (and thus wavelength) considered in this study, the two instruments are considered as co-located.

## 2.1 Data acquisition

The beat frequency between the two counter propagating gyrolaser beams is detected by a photodetector and acquired by the Virgo data acquisition system

at the rate of 5 kHz. The rotation rate signal is then reconstructed up to the frequency of 50 Hz by using the following procedure:

- the optical-beat signal  $v(t)$  is bandpass-filtered (with a digital first order Chebyshev filter) around the nominal Sagnac frequency within a bandwidth of about 90 Hz;
- the filtered signal and its Hilbert transform  $w(t)$  are combined to form the analytic signal  $z(t) = v(t) + jw(t)$ ;
- by expressing the analytic signal in the form  $z(t) = |z(t)|e^{j\psi(t)}$ , the instantaneous phase is estimated as  $\psi(t) \equiv 2\pi f_S t$  ;
- the instantaneous frequency  $f_S$ , connected to the rotation rate by the eq.(1) is finally estimated by calculating the derivative of the unwrapped instantaneous phase  $\psi$ ;
- the instantaneous frequency is down-sampled down to the final sampling frequency of 50 Hz and converted in rad/s by using eq.(2).

Signals from the accelerometer are acquired by Virgo’s internal acquisition system, and successively down-sampled to 50 Hz after appropriate low-pass filtering.

### 3 Data analysis

Data from “G-Pisa” represent the rotation rate  $\Omega_{\mathbf{x}}$  (tilt) around a horizontal vector  $\mathbf{x}$  which is oriented  $N19^\circ E$  (Fig. 1). The expected backazimuth (receiver-to-source angle measured clockwise from the N direction) of the Japan earthquake seismic wave is about  $36^\circ$ . Thus, the area vector of “G-Pisa” is misoriented by about  $73^\circ$  with respect to the rotation vector of the Rayleigh waves (Fig. 1). This oblique mounting implies that the recorded rotation rates can be significantly smaller than those predicted by theory.

Figure 2 shows the simultaneous recording of the vertical component of ground acceleration  $\ddot{u}_z$  and the horizontal rotation rate  $\Omega_x$  from “G-Pisa”. Overall, waveform morphology of the two time series are significantly similar. The main arrivals (P-, S- and Rayleigh waves) are clearly detectable on both recordings.

#### 3.1 Spectral Properties

Figures 3 and 4 illustrate the power spectral densities for the background noise preceding the earthquake, the P wave-train and its coda, and Rayleigh waves as recorded at the accelerometer and gyroscope, respectively.

Acceleration spectral peaks from both P- and Rayleigh waves span the 0.02 Hz - 3 Hz frequency band, and their energy is up to 4-5 orders of magnitude larger than that associated with background noise. Once compared to the noise spectrum, the rotational earthquake signal is much weaker. P-wave energy is at maximum 2 orders of magnitude larger than noise power over the 0.2-2 Hz

frequency interval; Rayleigh wave power is 2.5 orders of magnitude and less than one order of magnitude above the background level for the 0.03-0.1 Hz and 0.3-2 Hz frequency bands, respectively.

The frequency peak between 2 and 4 Hz is a persistent feature at both instruments. During the earthquake, its amplitude is slightly larger than during the preceding noise. This observation can be interpreted in terms of a site effect and/or resonance of the building, inducing narrow-band amplification of the earthquake signal. Alternatively, it could be that the microseismic noise (mostly of human origin) is stronger during the earthquake, simply because of the daily working cycle.

### 3.2 Relationships Between Ground Translations and Rotations

For a seismic wavefield defined by the displacement vector  $\mathbf{u}(u_x, u_y, u_z)$ , the relation between infinitesimal rotations  $\theta$  and translational motion is obtained through application of the curl operator as:

$$\begin{pmatrix} \theta_x \\ \theta_y \\ \theta_z \end{pmatrix} = \frac{1}{2} \nabla \times \mathbf{u} = \frac{1}{2} \begin{pmatrix} \frac{\partial u_z}{\partial y} - \frac{\partial u_y}{\partial z} \\ \frac{\partial u_x}{\partial z} - \frac{\partial u_z}{\partial x} \\ \frac{\partial u_y}{\partial x} - \frac{\partial u_x}{\partial y} \end{pmatrix} \quad (3)$$

Most of the experiments on the direct ring laser measurement of rotational ground motion are based upon sensors measuring rotation rates around a vertical axes (i.e.,  $\dot{\theta}_z = \Omega_z$ ). These devices are thus sensitive to transverse waves polarised on the horizontal (x,y) plane, that is S- and Love-waves. Under these conditions, [4] showed that the transverse ground acceleration  $\ddot{u}_T$  for Love waves is related to the vertical rotation rate  $\Omega_z$  by the simple relationship:

$$\ddot{u}_T = 2c_L \Omega_z, \quad (4)$$

where  $c_L$  is the local Love phase velocity. A similar expression is derived for the case of S-waves, with an additional factor accounting for the effects of non-horizontal incidence [13]. The above relationship has been exploited by several authors [10, 11, 14] to derive estimates of the medium velocity from Love waves dispersion characteristics.

By the same token, rotations around one of the two horizontal axes (let's say, the  $x$ -axis) requires wavetypes propagating along and transversely-polarised on the vertical ( $y, z$ ) plane. These are (i) P-wave, as a consequence of wave reflection-conversion at the free-surface; (ii) SV waves, and (iii) Rayleigh waves.

To the purpose of investigating the frequency-dependent performance of the rotational sensor, we focus on the ground rotation and vertical-component acceleration associated with the Rayleigh wave packet. We select these particular wave type and ground motion component as they are the ones exhibiting the largest amplitude, and hence the best signal-to-noise ratio. In the following, we thus proceed deriving a theoretical relationship between Rayleigh wave vertical

accelerations and rotations.

Assuming the surface corresponds to the  $xy$  plane, the zero traction boundary condition at the free surface implies that  $\sigma_{iz}$  ( $i = x, y, z$ ) = 0. Direct application of Hooke's law in a homogeneous, isotropic medium thus leads to:

$$\frac{\partial u_y}{\partial z} = -\frac{\partial u_z}{\partial y} \quad (5)$$

The Rayleigh-wave vertical displacement in a simple half-space Poisson solid is [15]:

$$u_z = f(y - c_R t) \quad (6)$$

where  $c_R$  is the Rayleigh wave phase velocity. From equations (3) and (5), the horizontal rotation rate is:

$$\Omega_x = \frac{\partial \dot{u}_z}{\partial y} = -\frac{1}{c_R} \ddot{u}_z \quad (7)$$

This latter relationship indicates that the amplitude ratio between the horizontal rotation rate and the vertical acceleration, is equal to the Rayleigh-wave phase velocity  $c_R$ . Note that this expression is slightly different from that reported in [4], who did not provide separate expressions for the two components of ground acceleration.

Eq. 7 is a simplification, valid for an infinite half-space. For the more realistic case of a layered Earth, one should account for the dispersion effects which imply a frequency dependence of  $c_R$ . In addition, interference of multiple, higher-order propagation modes should also be taken into account [5].

### 3.3 Correlation of Rotation Rates and Vertical Accelerations

In order to investigate the performance of the rotational sensor compared with the accelerometer, we superimpose vertical acceleration and rotation rate after filtering with a narrow bandpass (2-poles, zero-phase Butterworth with corner frequencies  $0.9 \times 1/T$  Hz and  $1.1 \times 1/T$  Hz, where  $T$  is the period in seconds). The selected signal segments are 1-hour-long, and they are centered at the predicted Rayleigh wave arrival ( $\approx 2400$ s after origin time). The procedure is iterated for 20 center periods spanning the 200s-10s period range. At periods longer than 100s, the results indicate excellent matching between ground rotation and acceleration (Fig. 5). At shorter periods (20s-100s), the two time series exhibit occasional phase differences, likely due to interference with late-arriving, scattered body waves. Nonetheless, the general waveform morphology is still significantly similar and the typical dispersive behavior of surface waves is clearly observed on both recordings.

For each frequency band, we quantify the time- and frequency-dependent similarity between rotation rate and vertical acceleration by sliding a time window of length twice the dominant period along the time-series, and calculate the zero-lag normalized correlation coefficient that is defined between -1 and 1.

Results are reported in the scaled-color image of figure 6, where the correlation coefficients are shown in their dependence on both time and periods.

From this latter data matrix, we then select the time intervals and frequency bands where the correlation coefficients are greater than an arbitrary threshold of 0.95. For those intervals, we take the median of the instantaneous (i.e., sample-by-sample) ratios between acceleration and rotation rate as an estimate of the amplitude relationships between the two quantities.

In general, the oblique mounting of “G-Pisa” with respect to the backazimuth implies that the measured rotations can be significantly smaller than those predicted by theory. Therefore, if the analyzed portion of the wavefield were purely composed by Rayleigh waves, then the acceleration / rotation amplitude ratio (eq. (??)) should always be greater than or equal to the local Rayleigh phase velocity. We thus use the AK135 Earth Model [16] to calculate the fundamental-mode, dispersion function for Rayleigh-wave phase velocity, and compare this function to the apparent velocities derived from the  $a_z/\Omega_x$  ratio.

The results, displayed in figure 7 indicate that the apparent velocities derived from the acceleration / rotation rate ratios are always greater than those predicted by the theory, thus confirming the interpretation of the ring-laser signal in terms of ground tilt associated with the passage of teleseismic, long-period Rayleigh waves.

## 4 Discussion and Conclusions

In this study, for the first time it is shown a remarkable consistency between rotational ground motions around a horizontal axis and vertical acceleration primarily quantified by the cross-correlation coefficient that is calculated in sliding time windows along the narrow-band filtered time series. Over the 100–200 s period range, the ring laser correlation with ground acceleration extends throughout the duration of the Rayleigh wave-packet. At shorter periods, the correlation between the two time series is much more discontinuous, pointing to a scattered wavefield constituted by the interference of multiple wave-types.

Apparent phase velocities estimated by taking the ratio of vertical acceleration and rotation rate, are compatible with the expected velocities assuming plane wave propagation, confirming recent results for vertically-oriented ring-laser gyroscopes [10, 11, 12]. This confirms that multi-component observations allow the estimate of wavefield properties (e.g. phase velocities, propagation direction) that otherwise can be achieved with high accuracy only through multichannel measurements. Our results open new perspectives for a wide range of applications for which high-sensitivity, very broad-band measurements of ground tilt are required. These include the surveillance of volcanic and geothermal areas, the monitoring of carbon dioxide capture and storage in geological structures, the control of oil and gas production plants.

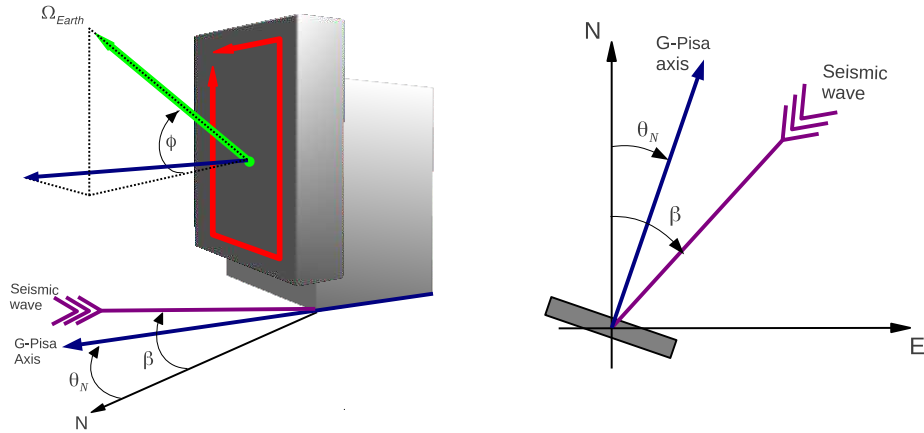


Figure 1: The “G-Pisa” apparatus in the vertical plane configuration: Left: schematics of the experimental apparatus. Right: top view. The reported angles are defined in the text.

## 5 Acknowledgements

We acknowledge F. Bosi, A. Gebauer, R. Hurst and U. Schreiber for the useful discussions. A. Velikoseltsev acknowledges the partial support from the Federal Targeted Program Scientific and scientific-pedagogical personnel of the innovative Russia in 2009-2013 of the Ministry of Education and Science of the Russian Federation.

## References

- [1] G. E. Stedman, Ring-laser tests of fundamental physics and geophysics, Rep. Prog. Phys. 60-6, 615, (1997)
- [2] V. Rautenberg, H.P. Plag, M. Burns, G.E. Stedman, H.U. Juttner, Tidally induced Sagnac signal in a ring laser, Geophys. Res. Lett., 24 (8), 893–896, (1997)
- [3] K.U. Schreiber, T. Klugel, G.E. Stedman. Earth tide and tilt detection by a ring laser gyroscope, J. Geophys. Res, 108 2132, (2003)



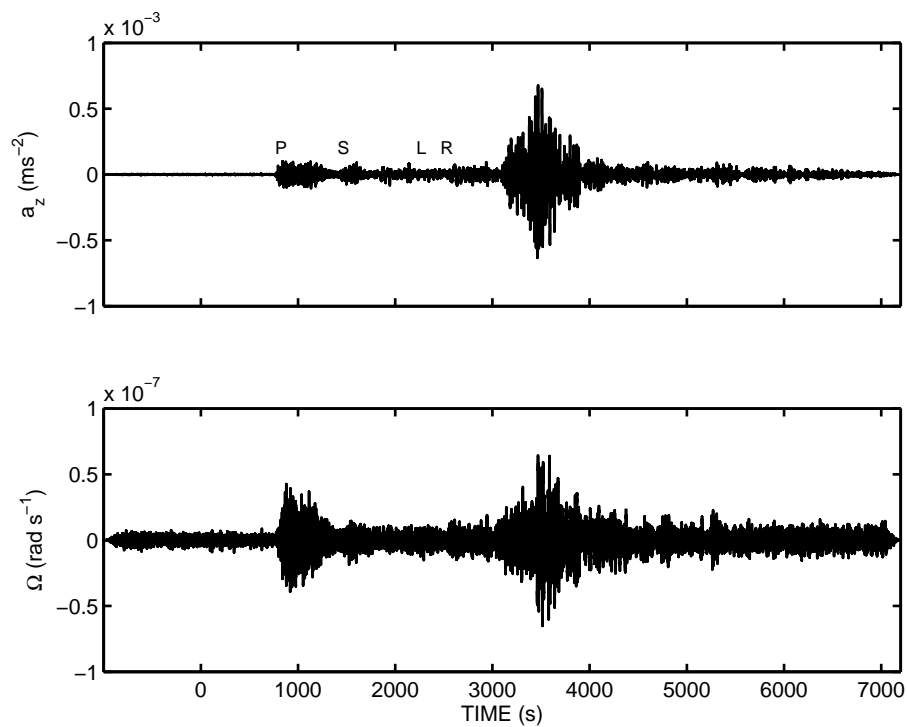


Figure 2: Recordings of vertical-component ground acceleration (top) and rotation rate (bottom) of the March 11, 2011,  $M_w=9$  Sendai-Honshu earthquake. Instruments are located within few meters inside the Virgo gravitational observatory laboratories. Traces have been band-pass filtered over the 100-s 1-s period range using a 2-pole, 2-passes Butterworth filter. The main seismic phases are marked; P,S,L and R correspond to direct P, S, Love and Rayleigh waves, respectively. Time 0 corresponds to the origin time of the earthquake (05:46:23 UTC).

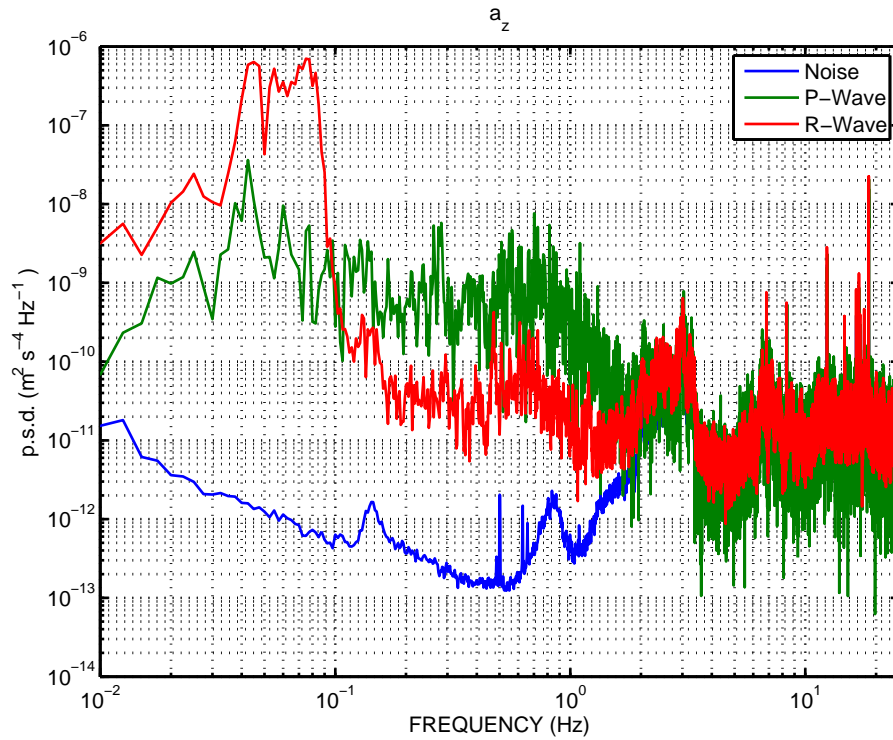


Figure 3: Power spectral estimates for the  $a(t)$  time series of a 5-hour-long noise window preceding the earthquake, a 600-s-long window encompassing the P-wave arrivals and coda, and a 1800-s-long window starting at the Rayleigh wave arrival. Power spectra are obtained by averaging and then squaring individual spectral estimates obtained over a 100-s-long window sliding by 50% of its length along the selected signal segments. Before transformation, individual signal slices were detrended, demeaned, and tapered by a 5% Tukey window.

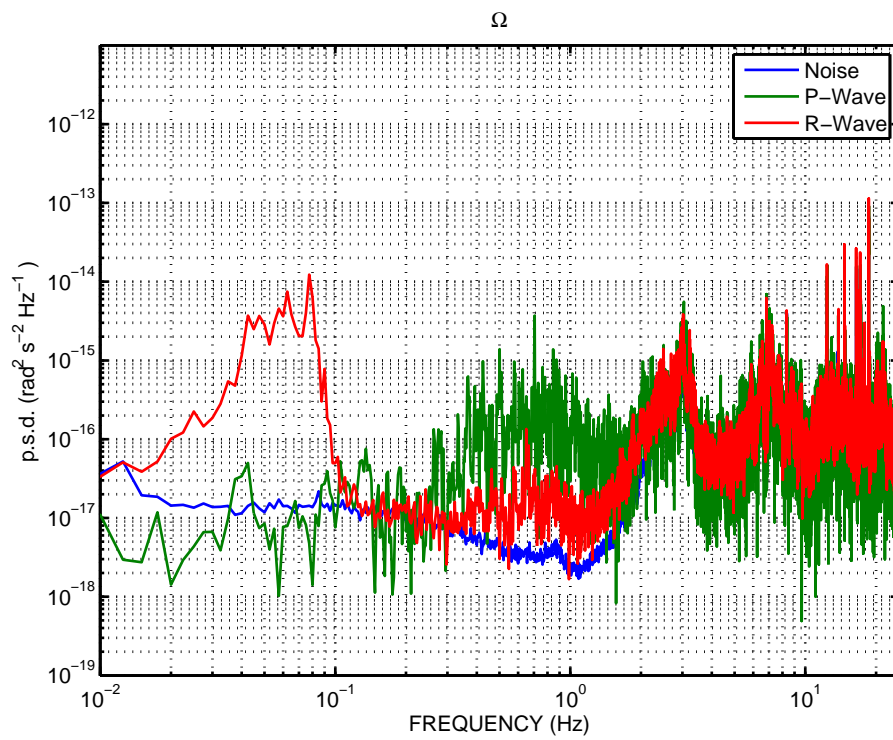


Figure 4: The same as in Figure 3, but for the Gyrolaser signal.

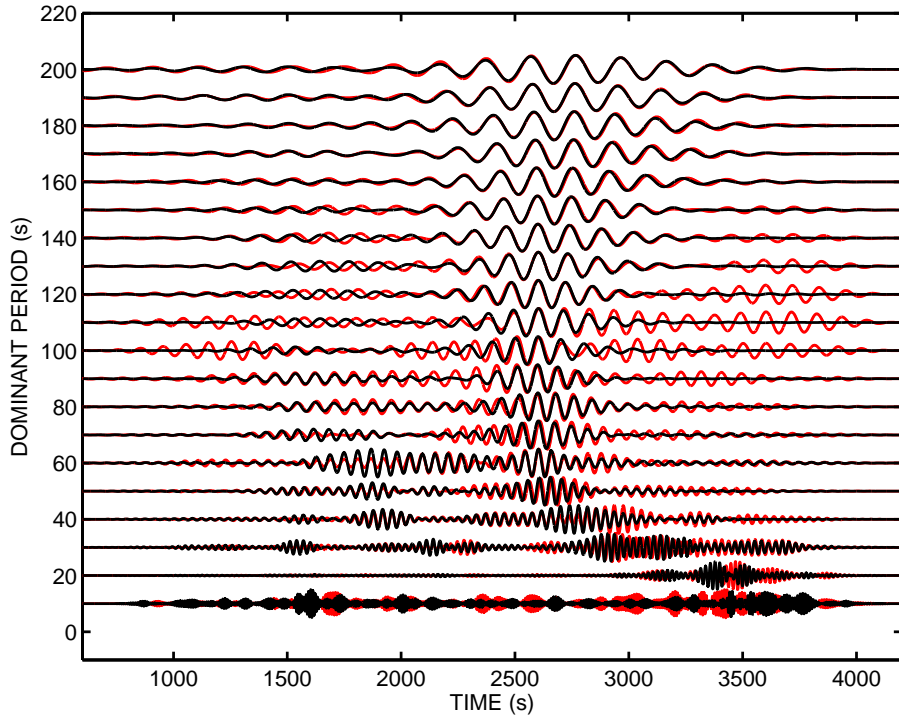


Figure 5: Superposition of vertical acceleration (black) and rotation rate (red) as a function of dominant period after narrow-band filtering. Each trace has been individually normalized. Signals start 1800s before the expected Rayleigh wave arrival; the time scale is referred to the event's origin time.

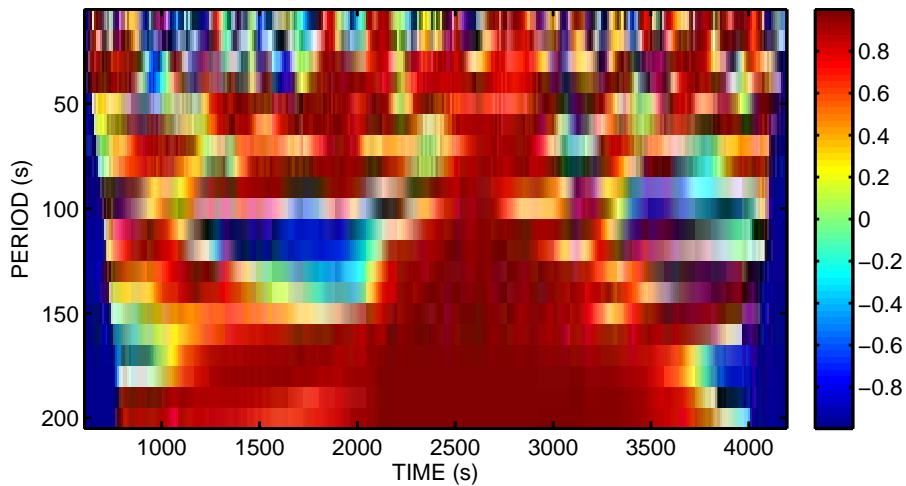


Figure 6: Normalized zero-lag correlation coefficient between vertical acceleration and rotation for the traces shown in Figure 5. For each frequency band, correlation has been computed over windows of length 2 dominant periods, sliding along the traces with 50% overlap.

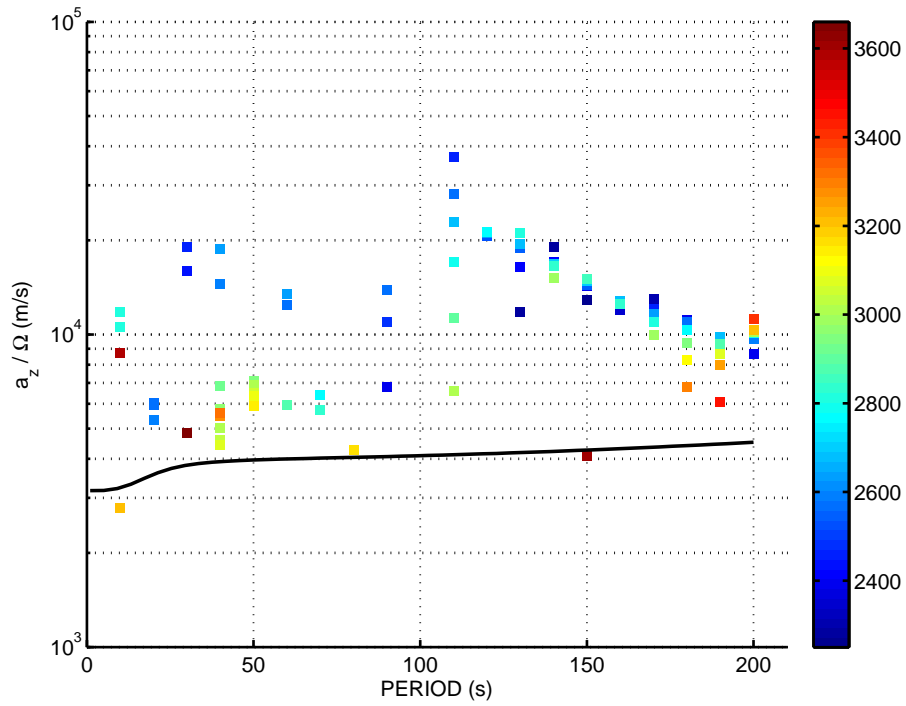


Figure 7: Amplitude ratios (apparent phase velocities) between vertical acceleration and rotation rate as a function of dominant period, for signal windows depicting zero-lag correlation greater than 0.95. The color of the symbols indicate the time location of the analyzed signal window, according to the color scale at the right. The black line marks the Rayleigh-wave phase velocity dispersion curve calculated for the AK135 velocity model. This line represents a lower bound on the possible  $a_z/\Omega$  ratios measured for waves propagating along different directions.

- [4] G.E. Stedman, Z. Li, and H.R. Bilger, Sideband analysis and seismic detection in large ring laser, *Appl. Opt.*, 34, 73907396, (1995)
- [5] D. Kurrle, H. Igel, A. M. G. Ferreira, J. Wassermann, U. Schreiber, Can we estimate local Love wave dispersion properties from collocated amplitude measurements of translations and rotations?, *Geophys. Res. Lett.* 37, L04307 (2010)
- [6] D.P. McLeod, G.E. Stedman, T.H. Webb, K.U. Schreiber, Comparison of standard and ring laser rotational seismograms, *Bulletin of the Seismological Society of America*, 88 (6), 1495–1503, (1998)
- [7] A. Pancha, T.H. Webb, G.E. Stedman, D.P. McLeod, K.U. Schreiber. Ring laser detection of rotations from teleseismic waves, *Geophys. Res. Lett.*, 27, 3553–3556, (2000)
- [8] J. Belfi, N. Beverini, F. Bosi, G. Carelli, A. Di Virgilio, D. Kolker, E. Maccioni, A. Ortolan, R. Passaquieti, F. Stefani, Performance of “G-Pisa” ring-laser gyro at the Virgo site, *Journal of Seismology* (2011).
- [9] K.U. Schreiber, G.E. Stedman, H. Igel, A. Flaws, Ring Laser Gyroscopes as Rotation Sensors for Seismic Wave Studies, *Earthquake Source Asymmetry, Structural Media and Rotation Effects*, 377–390, (2006)
- [10] H. Igel, K.U. Schreiber, A. Flaws, B. Schuberth, A. Velikoseltsev, A. Cochard. Rotational motions induced by the M8. 1 Tokachi-oki earthquake, September 25, 2003, *Geophysical Research Letters*, 32 (8), (2005)
- [11] H. Igel, A. Cochard, J. Wassermann, F. Asher Flaws, U. Schreiber, A. Velikoseltsev and N. Pham Dinh, Broad-band observations of earthquake-induced rotational ground motions, *Geophys. J. Int.*, 168, 182196, (2007)
- [12] A. Cochard, H. Igel, B. Schuberth, W. Suryanto, A. Velikoseltsev, U. Schreiber, J. Wassermann, F. Scherbaum, and D. Vollmer, Rotational motions in seismology: theory, observation, simulation, R. Teisseyre, M. Takeo and E. Majewski, *Earthquake source asymmetry, structural media and rotation effects*, Springer Verlag, Berlin Heidelberg. 7, 62, 72, (2006)
- [13] H. Li, L. Sun, and S. Wang, Improved approach for obtaining rotational components of seismic motion, *Transactions, SMiRT16*, Washington DC, (2001)
- [14] Takeo M., Rotational Motions Observed during an Earthquake Swarm in April 1998 Offshore Ito, Japan, *BSSA*, 99 (2B), 1028, (2009)
- [15] T. Lay, T. C. Wallace, *Modern global seismology*, Academic Press (San Diego), (1995)
- [16] B.L.N. Kennett, E.R. Engdahl and R. Buland, Constraints on seismic velocities in the Earth from traveltimes, *Geophys. J. Int.*, 122, 108-124, (1995)